Memorias del Congreso Nacional de Control Automático
ISSN: 2594-2492

Gravity Compensation Control of a 2-DOF Spherical Parallel Manipulator ⋆

Azgad Casiano-Ramos * **Aldimir Mora-Sota** **
Hugo G. Gonzalez-Hernandez *** **Antonio Benítez-Ruiz** ****
María D. Guevara-Espinosa * **Jesús M. Muñoz-Pacheco** *

* *Benemérita Universidad Autónoma de Puebla. Av. Sn. Claudio S/N. Cd. Universitaria, Pue. 72570, México (e-mail: jesusm.pacheco@correo.buap.mx).*
** *CEDVA Professional Working Center. 33 Sur 23011. Pue. 72453, México.*
*** *Escuela de Ingeniería y Ciencias. Tecnológico de Monterrey. Ave. Eugenio Garza Sada 2501. Monterrey, N.L., México.*
**** *Universidad Politécnica de Puebla, Blvd. Cholula-Huejotzingo Km. 5, Cholula, Pue. Mex., C.P. 72640, México.*

Abstract: In this work, a gravity compensation controller for a 2-DOF spherical parallel wrist with a camera mounted on the end effector is derived in order to reduce the joints positioning error given by a PD controller during camera orientation. Here, the camera body is considered as a 2D pendulum with origin at the sphere center and referenced to the end effector stable plane. Thus, the gravity compensation torques for the joints are obtained by following the Euler-Lagrange methodology through inverse kinematics. Significant reduction in magnitude and variability of the joints positions errors demonstrates the enhanced performance and validity of the present approach. Experimental controller implementation is described and a discussion on the results is given.

Keywords: Visual tracking, parallel eye robot, dynamic control.

1. INTRODUCTION

Parallel Wrists (PW) are some kind of spherical parallel manipulators arising at the middle of the 90's (Gosselin and Hamel, 1994). We can describe them as mechanisms where each one of the mobile links rotates around an stationary common point. As a consequence of this, the movement of every point on the link is restricted by a sphere (Wu (2006)). Although in recent years special attention has been given to the study of this kind of mechanisms, there is a lack of literature focused on this topic, and research on their simulation and control is almost null. There have been reported a variety of applications including pointing systems (Samson et al. (2006)), CNC cutting procedures (Ur-Rehman et al. (2009)), haptic minimally invasive surgery (Chaker et al. (2012)), between others. Actually, the most popular application of PWs is the so-called Agile Eye or 3 DOF PW (Gosselin and Hamel (1994)), (Gosselin et al. (1996)). Been such works the most important within the limited information, those are seminal papers for most of the prototypes developed nowadays. Some of the most relevant research about spherical PWs up to date are summarized in Table 1.

Table 1. Some relevant studies on spherical PWs.

Author (Year)	Research area
Gosselin and Hamel (1994)	Kinematics, Mechanical design & Dynamics
Alizade et al. (1994)	Kinematics
Gosselin et al. (1996)	Kinematics, Mechanical design Dynamics & Control
Di Gregorio (2002)	Structural Synthesis
Bonev et al. (2006)	Assembly modes
Samson et al. (2006)	Vision and control
Bai et al. (2012)	Forward Displacement Analysis

2. 2-DOF SPHERICAL PARALLEL MANIPULATOR

The spherical 2-DOF PW under study, is a simpified version of the 3-DOF Agile Eye (Bonev et al. (2006)). This is a mechanism used to pose a body in a 3D space using only a couple of independent rotations of a mobile platform, around a fixed point or base. In Fig. 1 it can be observed the mechanical system reference plane according to Ur-Rehman et al. (2009). Forward kinematics are straightforward obtained from here. Input angles θ_1 and θ_2 are the rotational displacements of each one of the motors; and orientataion angles of the end-effector are the deduced φ_1 (roll) and φ_2 (pitch) angles.

⋆ This work was partially supported by CONACYT. Scholarship No. 493227.

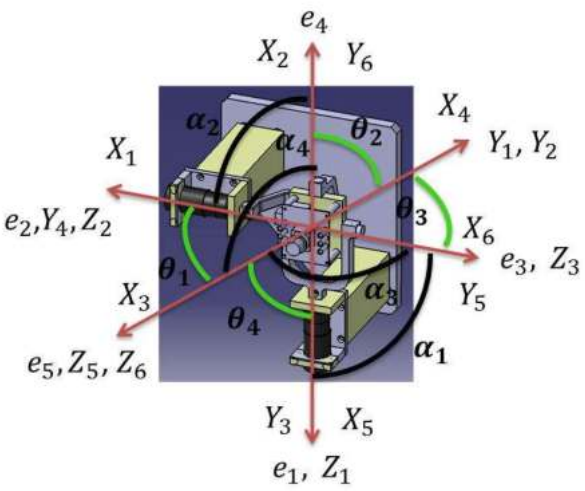

Fig. 1. 2 DOF PW reference frame.

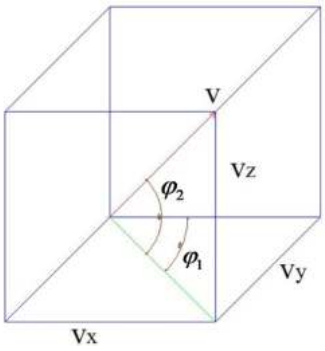

Fig. 2. Orientation of vector V.

In Fig. 1 e_i is a unit vector associated to each joint and aligned with the Z_i axis of an R_i reference frame; α_i denotes the angle between e_i and e_{i+2} for $i = 1 \dots 4$; e_2 is defined to lie in the X_1Z_1 plane of R_1 and e_1 is defined to lie in the X_2Z_2 plane of R_2; and α_i, θ_i are the Denavit-Hartenberg parameters of frame R_i obtained with respect to the R_{i-2} for $i = 3, 4, 5, 6$. In order to obtain the desired position and orientation of the end-effector, components V_x, V_y and V_z defining vector V are required (see Fig. 2). Equations 1 are used to define the orientation of such a vector (Samson et al. (2006)).

$$\begin{aligned} \varphi_1 &= \theta_1 \\ \varphi_2 &= \arctan\left[\frac{\tan\theta_2}{\cos\theta_1}\right] \end{aligned} \tag{1}$$

In Fig. 3 an exploded view of the mechanism is shown. Subsequent experiments are based on this schematic. The built prototype is shown in Fig.4.

3. CONTROL SYSTEM IMPLEMENTATION

Motion control system for the two axes of the robot was implemented by using the *SOFT*DMC firmware for motion control from Mesa Electronics (Mesanet (2019)). *SOFT*DMC is a firmware running over I/O boards based on FPGA for autonomous operation. That is, CPU, RAM, ROM and a real time events logic are programmable and reside in just one FPGA; I/O ports of the FPGA

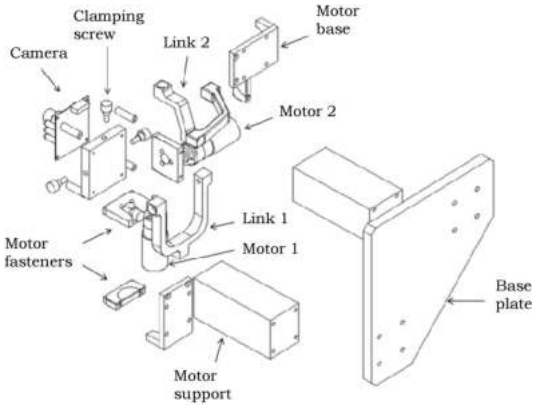

Fig. 3. Mechanical design exploded.

Fig. 4. Experimental 2 DOF robot prototype.

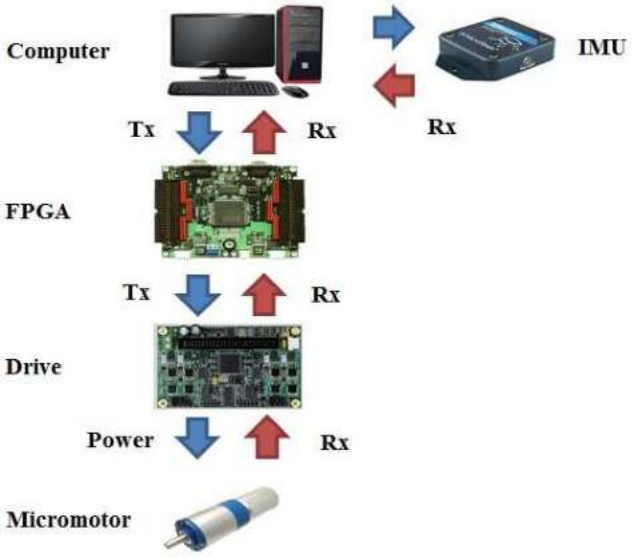

Fig. 5. Motion control system interconnections.

can be directly connected to power and DAQ boards and control variables can be manipulated from a host through an intelligent serial interface. A maximum of 4 to 8 independent real-time PID controllers are available on a single FPGA card, depending on motor commutation technology.

An interconnection scheme of the robot control system components is depicted in Fig. 5 and the functions of each individual element are summarized in Table 2.

Table 2. Control system components.

Component	Model	Function
Dual H-Bridge	Mesa 7I40	Driver
FPGA Card	Mesa 7I60	HW Controller
Firmware	*SOFT*DMC	DSP Controller
DC Micromotor	Faulhaber 2232	Actuator
Incr. Encoder	Faulhaber IE2-512	Position Sensor
3-Axial IMU	XSENS 3DM-GX1	Orientation Sensor
Core 2 Duo PC	Vecow VSM-200	Host Controller

In *SOFT*DMC the joint-level control loop is a PID type that can be augmented with velocity (KF1), acceleration (KF2) and torque (KK) feedforward terms. Equation 2 describes the PID controller as implemented by *SOFT*DMC, where KP, KI, KD denote the proportional, integral and derivative gain terms. A block diagram of the control system in terms of the *SOFT*DMC variables is represented in Fig. 6.

$$DRIVE = KP(DESPOS - ENCP) + KI \sum (DESPOS - ENCP)\Delta t + KD(DESVEL - ACTVEL) + KF1(DESVEL) \quad (2)$$

The sampling period of the control board was configured to be 20 KHz for each of the two axes. For the host, the real time program execution was obained by using Linux 11.04 with TAI 3.9 complement. A serial communication running at 230.4 KBaud allowed us to refresh the feedback position and reading commands at every 1000 μs. The set of libraries and functions for coding/decoding and communicating frames with *SOFT*DMC were implemented using ANSI C. A set of programs implemented in C/C++ were used to read data from the RS-232 inertial sensor port and to do visual object tracking from analog video signals.

4. CONTROLLER DESIGN

By considering the PW camera manipulator as an ideal 2D pendulum of length l with origin at the center of the sphere, and by using the notation C_β and S_β for the cosine and the sine of a given angle β, respectively, the following kinematic relation of the spherical coordinates (ϕ_1, ϕ_2) to the end effector position (x, y, z) holds:

$$\begin{bmatrix} x \\ y \\ z \end{bmatrix} = \begin{bmatrix} lC_{\phi_1}S_{\phi_2} \\ lS_{\phi_1}S_{\phi_2} \\ lS_{\phi_2} \end{bmatrix} \quad (3)$$

Thus, relating (3) to (1) a gravity torque compensanting controller can be obtained by following the Euler-Lagrange methodology as follows:

$$\frac{\partial \mathcal{L}(\theta, \dot{\theta})}{\partial \theta_1} = mglC_{\theta_1}Sv + mglC_{\theta_1}C_v \frac{\sec\theta_1 \tan\theta_1 \tan\theta_2}{1+v^2} \quad (4)$$

$$\frac{\partial \mathcal{L}(\theta, \dot{\theta})}{\partial \theta_2} = mglS_{\theta_1}C_v \frac{\sec\theta_1 \sec^2\theta_2}{1+v^2} \quad (5)$$

where:

$$v = \arctan\left(\frac{\tan\theta_2}{\cos\theta_1}\right)$$

and $\mathcal{L}(\theta, \dot{\theta})$ is the Lagrangian of the generalized coordinates $\theta = [\theta_1 \quad \theta_2]^T$ and $\dot{\theta} = [\dot{\theta}_1 \quad \dot{\theta}_2]^T$. By adding a PD term to each control torque, the gravity compensation controller for the 2 DOF parallel mechanism is given by:

$$\tau_1 = k_{p_1}\tilde{\theta_1} + k_{v_1}\dot{\tilde{\theta}_1} + mglC_{\theta_1}Sv + mglC_{\theta_1}C_v \frac{\sec\theta_1 \tan\theta_1 \tan\theta_2}{1+v^2} \quad (6)$$

and

$$\tau_2 = k_{p_2}\tilde{\theta_2} + k_{v_2}\dot{\tilde{\theta}_2} + mglS_{\theta_1}C_v \frac{\sec\theta_1 \sec^2\theta_2}{1+v^2} \quad (7)$$

5. EXPERIMENTAL SETUP AND RESULTS

A prototype of a 2 DOF PW was designed and machined and the computerized control described above was implemented using Faulhaber precision micromotors, a MESA Electronics FPGA board and a Core 2 Duo @ 2.2 GHz running a vision system over Linux RTAI. Three experiments are depicted here using a PID controller.

5.1 Angular position control

The first experiment conducted with the prototype was the axes PID position control in the joint space. The objective was to evaluate the ability of the servomechanism to respond to ramp and step-type inputs. As it can be seen in Fig. 7, a rising time of 3 ms was obtained for a step reference of 20 degrees. The error magnitude for the two robot axes with respect to the reference position is shown in Fig. 8. The steady state error was kept below or equal to 0.0125 degrees for both cases. Note that this experiment just give us information about the real motion of the joints, not about the overall displacement of the mechanism.

In order to explore tracking properties of the system, a second experiment consisted on stablishing the trajectory $20*(1-\cos(20t))$ for both axes. Tracking response is shown in Fig. 9. Fig. 10 shows the tracking error for link 1.

5.2 Forward and inverse orientation control

Several tests were done with the mechanism by using an Inertial Measurement Unit (IMU) posed at the end-effector, making coincide its roll and pitch axes with the corresponding axes of the mechanism. First test consisted on programming a home-posing routine of the mechanism using orientation feedback from the IMU. A proportional control law for velocity (equation 8) was implemented in order to achieve orientation of the end-effector in coordinates $(roll, pitch) = (\varphi_1, \varphi_2) = (0, 0)$.

$$u_i = -k_p\varphi_i^{IMU} \qquad [deg/s] \quad (8)$$

Since the IMU gives absolute coordinates, it is worth to mention that the mechanism must be located over a balanced and straighten bench in order to obtain correct results for the following experiments.

The next experiment consisted on validating the inverse kinematic equations given in Caron (1997). Once at home

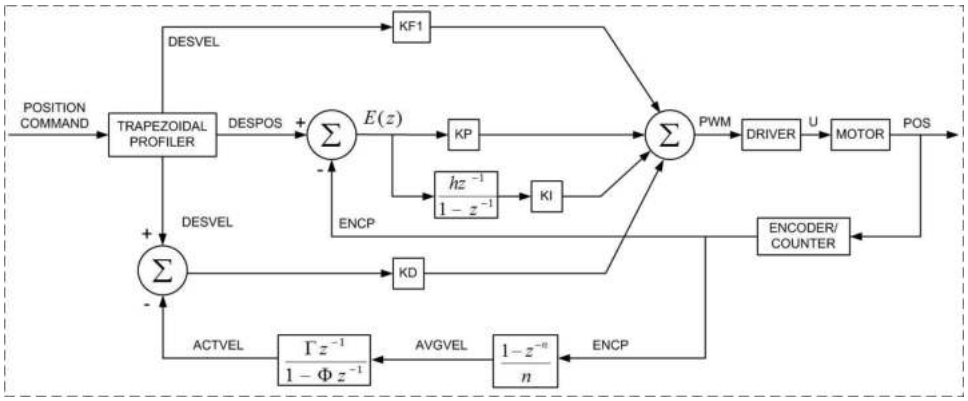

Fig. 6. System block representation of *SOFT*DMC real time motion control loop.

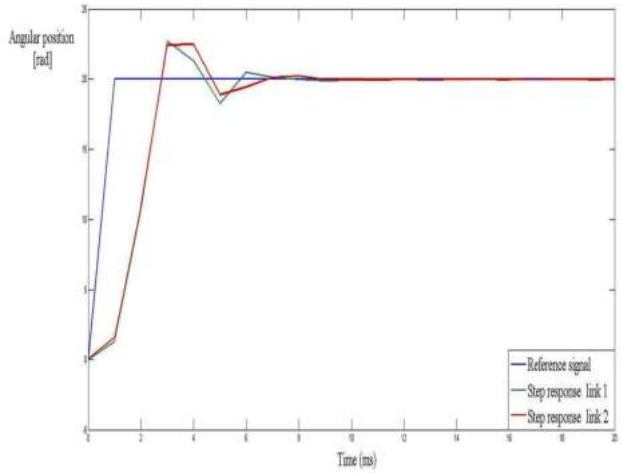

Fig. 7. Step response of PID controller.

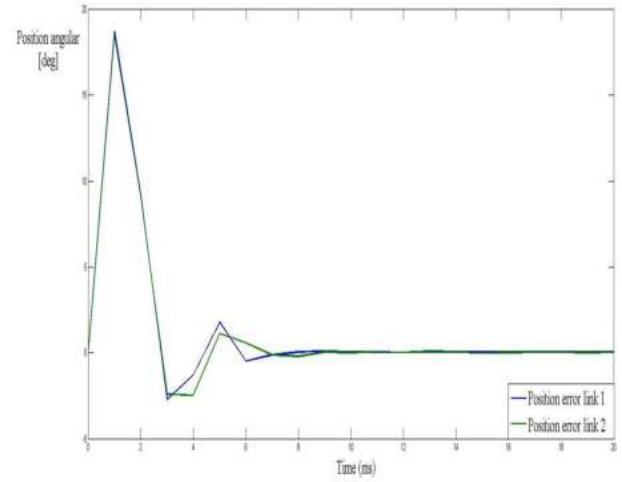

Fig. 8. Step response error of PID controller.

position, the desired coordinates $(roll, pitch) = (-10, 5)$ of the mechanism were proposed and joint position commands were generated $(\theta_1, \theta_2) = (-10, 5.07)$. Results are shown in Fig. 11. Forward kinematics was validated transfering the steady state IMU coordinates to obtain again the estimated coordinates $(\hat{\theta}_1, \hat{\theta}_2)$. Position errors were

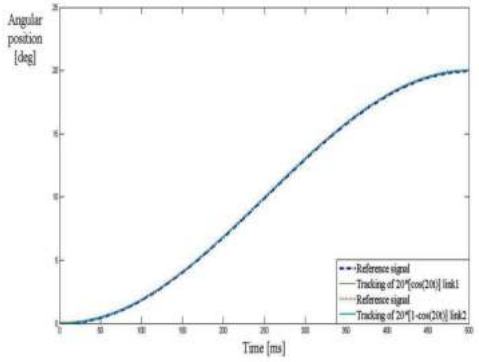

Fig. 9. Tracking response of PID controller for S-curve.

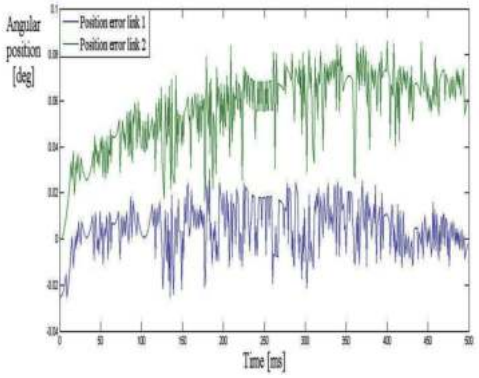

Fig. 10. Tracking error of PID controller.

observed in the prototype and they coincide with a previously reported work (Chaker et al. (2013)), these errors are associated to imperfections on machining procedures and manufacture of the non-actuated joints.

5.3 Tracking using vision system

A third experiment was conducted for tracking of a moving object recognized using information from a vision system. Roll and pitch coordinates computed by the vision system were directly transfered to variables θ_1 and θ_2. Tracking results and error are plot in Figs. 12 and 13, respectively. It can be observed a greater tracking error, we attribute this error augmenation , in part, due to a certain delay in the communication with the vision system interface,

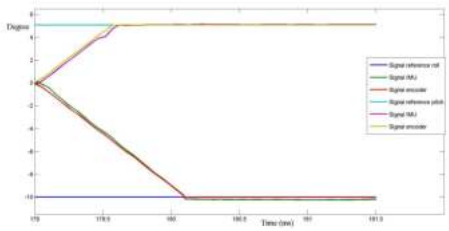

Fig. 11. Inverse orientation response of the mechanism.

and on the other hand, due to the friction of the axes of the mechanism, which was not considered by the PID controller. This error increment was the motivation for the authors to apply a more robust control technique.

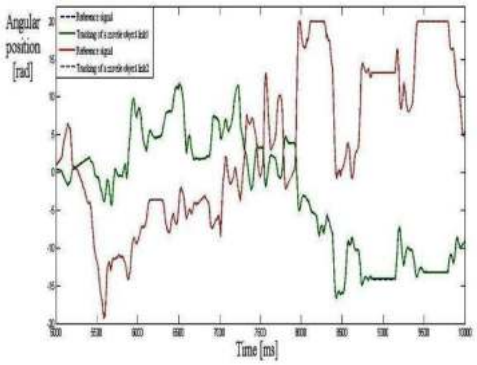

Fig. 12. Vision system tracking response of PID controller.

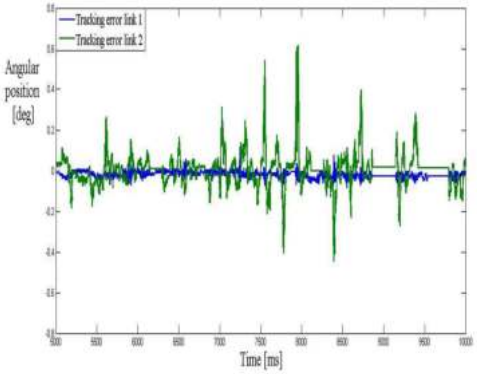

Fig. 13. Vision system tracking error of PID controller.

5.4 Testing of the gravity compensation controller

The controllers (4) and (5) were implemented as:

$$\tau_1 = k_{p_1}\tilde{\theta_1} + k_{v_1}\dot{\tilde{\theta}_1} + 6400C\theta_1 Sv + 6400C_{\theta_1}C_v\frac{\sec\theta_1\tan\theta_1\tan\theta_2}{1+v^2}$$

$$\tau_2 = k_{p_2}\tilde{\theta_2} + k_{v_2}\dot{\tilde{\theta}_2} + 6750S_{\theta_1}C_v\frac{\sec\theta_1\sec^2\theta_2}{1+v^2} + 735(\sin(\theta_2 - \theta_{2d}))$$

Where the last term compensates for the initial offset of θ_2 when the pendulum is at its equilibrium (i.e., $\theta_{2(eq)} = \theta_{2d}$). k_{p_i} and k_{v_i} correspond to the KP and KD gains in the *SOFT*DMC controller, respectively. Now, the control objective was to follow an S-bell function as that of figure 14. Comparative results between the PID and the proposed gravity compensation controller are shown in Figures 15 and 16. As it can be seen, an error reduction of about 0.08 to 0.04 degrees was obtained during the acceleration/decceleration phase, while a free of oscillations position response behavior was obtained during the constant velocity part.

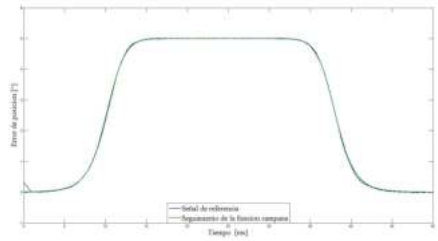

Fig. 14. S-curve to test response of PID and PD plus gravity compensation controllers.

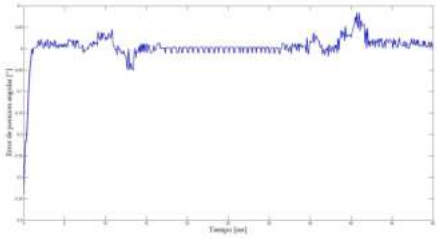

Fig. 15. Error response of PID control on tracking an S-curve on the 2 DOF parallel robot.

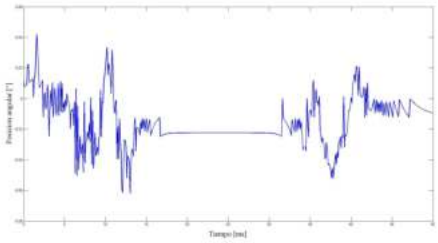

Fig. 16. Error response of PD plus gravity compensation control on tracking an S-curve with the 2 DOF parallel robot.

6. DISCUSSION

A gravity compensation controller for the a 2 DOF spherical manipulator was proposed through the Euler-Lagrange methodology. Also an electromechanical prototype was designed and built based on the 2 DOF parallel wrist configuration proposed by Gosselin. Experimental tests were conducted for testing individual motion control of the robot joints and coordinated control during simple vision coordinate tracking experiments. Results indicate a significant improvement on the desired quantitative and qualitative robot response and the validity of the proposed control methodology for the present robot configuration.

ACKNOWLEDGEMENTS

Authors want to thank Dr. Leopoldo Altamirano Robles former Director of INAOE mexican research institute and to M. Sc. Iván Olivera Romero, INAOE Director of Technology, for the facilities given to develop this project at the INAOE Computer Vision Laboratory.

REFERENCES

Alizade, R., Tagiyev, N., and Duffy, J. (1994). A forward and reverse displacement analysis of an in-parallel spherical manipulator. *Mechanism and Machine Theory*, 29, 125–137.

Bai, S., Hansen, M.R., and Angeles, J. (2012). Robust forward-displacement analysis of spherical parallel robots. *Mechanical Systems and Mechatronics*, 55, 2204–2216.

Bonev, I., Chablat, D., and Wenger, P. (2006). Working and assembly modes of the agile eye. *IEEE International Conference On Robotics And Automation*.

Caron, F. (1997). *Analyse et conception d'un manipulateur parallèlele sphérique à deux degrés de liberé pour l'orientation d'une caméra*. Master's thesis, Laval University.

Chaker, A., Mlika, A., Laribi, M.A., Romdhane, L., and Zeghloul, S. (2012). Synthesis of spherical parallel manipulator for dexterous medical task. *Frontiers of Mechanical Engineering*, 7, 150–152.

Chaker, A., Mlika, A., Laribi, M.A., Romdhane, L., and Zeghloul, S. (2013). Clearance and manufacturing errors effects on the accuracy of the 3-rcc spherical parallel manipulator. *Robot Design, Dynamics and Control*, 544, 27–34.

Di Gregorio, R. (2002). *Structural Synthesis*, volume 20 of *Solid Mechanics and Its Applications*. Springer.

Gosselin, C.M. and Hamel, J.F. (1994). The agile eye: a high performance three-degree-of-freedom camera-orienting device. *Proceedings of the IEEE International Conference on Robotics and Automation*.

Gosselin, C.M., St. Pierre, E., and Gagné, M. (1996). On the development of the agile eye. *IEEE Robotics & Automation Magazine*.

Mesanet (2019). URL `http://www.mesanet.com/`.

Samson, E., Laurendeau, D., Parizeau, M., Comtois, S., Allan, J.F., and Gosselin, C.M. (2006). The agile stereo pair for active vision. *Springer-Verlag Machine Vision and Applications*, Volume 17,.

Ur-Rehman, R., Caro, S., Chablat, D., and Wenger, P. (2009). Kinematic and dynamic analysis of the 2-dof spherical wrist of orthoglide 5-axis. *3rd International Congress Design and Modelling of Mechanical Systems CMSM'2009*.

Wu, H. (ed.) (2006). *Parallel Manipulators Towards New Applications*. I-Tech Education and Publishing.

